Russian Journal of Earth Sciences

What Should We Know to Predict Geomagnetically Induced Currents in Power Transmission Lines?

V. A. Pilipenko[*,1,2], **O. V. Kozyreva**[2], **V. B. Belakhovsky**[3], **Ya. A. Sakharov**[3], **and V. V. Selivanov**[4]

[1]Geophysical Center of Russian Academy of Sciences, Moscow, Russia
[2]Schmidt Institute of Physics of the Earth, Moscow, Russia
[3]Polar Geophysical Institute, Apatity, Russia
[4]Institute of Northern Energetics, Apatity, Russia
* **Correspondence to:** Vyacheslav Pilipenko, space.soliton@gmail.com

Abstract: This review considers several issues of space weather studies that are directly related to the problem of geomagnetically induced current (GIC) excitation in the power line transmission systems. Expectations to reduce the damage to technological systems from space weather were related with elaboration of models capable of real-time predictions of electromagnetic disturbances at the Earth's surface. However, the examination of the feasibility of the MHD simulation to predict the level of geomagnetic field variability, and consequently GICs, during the May 27–28, 2017 storm showed that the modeling reasonably well reproduced the global magnetospheric parameters, but the predicted magnetic field variability dB/dt has turned out to be more than order of magnitude less than that observed. The reason is the inability of current global MHD models to adequately predict the fine structure of the storm/substorm – Pi3 disturbances, and consequently GICs that they drive. Moreover, impulsive disturbances such as Pi3 pulsations demand a special tool for their analysis. Data processing technique for a 2D network of magnetic stations has to be elaborated to automatically recognize eddy current structures in the ionosphere and estimate their characteristics. The proposed technique applied to Pi3 pulsations on March 17, 2013 revealed that each vortex caused a disturbance of the vertical magnetic component Z and GIC burst up to ~ 100 A. The efficiency of GIC generation by different types of magnetic storms must be examined. For that it is necessary to compare GIC responses to storms caused by coronal mass ejection and by corotating interaction region, and to estimate the normalized GIC-effectiveness of each storm. The excitation rate of GIC during storms may be associated with the occurrence of mesoscale current vortices.

Keywords: magnetic storm, substorms, magnetic impulsive events, ionospheric vortex, geomagnetically induced currents, Pi3 pulsations, power transmission lines.

Citation: Pilipenko, V. A., O. V. Kozyreva, V. B. Belakhovsky, Ya. A. Sakharov, and V. V. Selivanov (2024), What Should We Know to Predict Geomagnetically Induced Currents in Power Transmission Lines?, *Russian Journal of Earth Sciences*, 24, ES6006, EDN: VETPKC, https://doi.org/10.2205/2024es000954

Research Article

Received: 3 August 2024
Accepted: 21 November 2024
Published: 30 December 2024

Introduction

One of the most harmful factors of space weather for technological systems is electric geomagnetically induced currents (GICs) caused by rapid changes of the geomagnetic field **B**, i.e., large values of $d\mathbf{B}/dt$. GICs associated with intense magnetic disturbances were found to be dangerous for various technological systems, causing overheating of industrial transformers, imbalance of power line transmission, malfunction of railway equipment, disruption of communication cables, reduction of the lifetime of pipelines, etc. (see references in review [*Pilipenko*, 2021]). For example, the catastrophe of the Hydro Quebec energy system was caused by a storm with dB/dt ~ 480 nT/min [*Kappenman*, 2005], although the impact of GIC on power lines was also observed at much lower dB/dt ~ 100 nT/min

[*Pirjola et al.*, 2005]. The highest risk of GIC may be related not directly to global magnetic storm/substorms processes with enormous energy yield, but to more local and rapid processes. Such meso-scale processes embedded into storm/substorm evolution can be the actual drivers of GIC bursts [*Belakhovsky et al.*, 2019]. The abrupt disturbances that appear in magnetometers during nighttime may be associated with substorm onsets, isolated magnetic impulse events with a duration of ~ 5–15 min [*Engebretson et al.*, 2020], quasi-periodic series of such impulses – geomagnetic Pi3 pulsations (quasi-periods around 5–20 min) [*Kozyreva et al.*, 2019; *Yagova et al.*, 2021], and quasi-monochromatic Pc5 pulsations [*Heyns et al.*, 2021]. Some authors introduce in the Pi3 frequency band additional subclasses of ultra-low-frequency (ULF) pulsations, such as Ps6 or Pc6, but for brevity we call all of them as Pi3 pulsations. Though the power of such impulsive processes is much lower than the magnetic storm power, the rapidly varying electromagnetic fields of these events can induce a significant GIC [*Apatenkov et al.*, 2020; *Ngwira et al.*, 2018; *Viljanen and Pirjola*, 1994]. In general, meso-scale disturbances on short timescales may be considered as a kind of the space weather "tornadoes". Any progress in building the effective system for the GIC prediction demands the solution of several mutually related problems on these "tornadoes". Here we consider several issues of the fine time-spatial structure of storm/substorm and discuss some efforts in resolving these issues.

Practical steps taken by the international geophysical community to reduce the damage to technological systems from space weather include the development of numerical models capable of real-time predictions of geoeffective electromagnetic disturbances at the Earth's surface [*Pulkkinen et al.*, 2013]. These models are based on the physical principles of the solar wind interaction with the Earth's magnetosphere and directly solve equations representing the underlying physical processes in the solar-terrestrial system using the driving conditions in the interplanetary space [*Gombosi et al.*, 2021]. Special attention is to be paid to the capabilities of the current models to adequately predict $d\mathbf{B}/dt$ values, i.e., fast fluctuations of the magnetic field, which are the main indicator of the appearance of dangerous levels of GIC. Desirably, the modeling results are to be compared not just with GIC proxy $d\mathbf{B}/dt$, but with actual observations of GIC in power transmission line.

It has become a necessity to find an adequate tool to reveal the temporal-spatial features of geomagnetic variations most responsible for the GIC generation [*Dimmock et al.*, 2021]. The energy transfer of electromagnetic disturbances from the Earth's magnetosphere to the ionosphere occurs mainly due to the field-aligned currents (FACs), so geomagnetic impulses can be driven by localized FAC. Such a system of eddy Hall currents driven by FACs produces meso-scale magnetic disturbances. The eddy ionospheric currents can have very different spatial-time scales, depending on the type of magnetospheric disturbance. The ability to automatically recognize localized vortex structures and determine their parameters using magnetometer data is an extremely important task.

Standard wave analysis tools (Fourier decomposition into harmonic waves, description of space structure with a set of plane harmonics, etc.) cannot be applied for the consideration of impulsive disturbances. Commonly, the presence of vortex structures in geomagnetic disturbances is determined visually from the equivalent ionospheric current pattern. More advanced technique is the spherical elementary current system (SECS) approach based on data from 2D magnetometer array [*Amm and Viljanen*, 2014]. Additionally, a new method was proposed in [*Chinkin et al.*, 2020], which makes it possible from data of 2D magnetometer network to automatically determine several simultaneous vortex structures and their instant characteristic parameters. Such methods should be applied to a study of geomagnetic events which produce a very intense burst of GIC.

Magnetic storms are considered a major risk factor for power systems at high latitudes. Two sources of magnetic storms are Coronal Mass Ejections (CMEs) emanating plasma clouds, and Corotating Interaction Regions (CIRs) created by high-speed solar wind streams from coronal holes. The question arises about the efficiency of the GIC generation by different types of magnetic storms.

Despite an enormous database of observations with a flotilla of satellites, extensive arrays of ground magnetometers and ionosphere sounders, and Sun imagers, some key questions related to the GIC excitation are still unsolved. These questions are related to the feasibility of global computer modeling to resolve meso-scale processes in the near-earth space, the availability of adequate tools for detection and analysis of meso-scale structures of magnetic storm/substorm, and the determination of key factors that control the GIC-effectiveness of different types of magnetic storms. In this review we'd like to draw the attention of the space community to these problems and present some preliminary steps in resolving these issues.

Prediction of Space Weather Hazard With MHD Modeling

Permanent monitoring of the interplanetary space upstream the Earth opens a principal possibility to construct a GIC forecast with a horizon of about one hour [*Morley*, 2020]. A promising forecast method combines global space weather models and simulations of near-surface electromagnetic fields [*Pulkkinen et al.*, 2007; *Zhang et al.*, 2012]. The input parameters of such models are satellite data on the solar wind plasma, interplanetary magnetic field (IMF), and solar radio flux F10.7 transmitted in real time from satellites at ~ 200 Earth radii (R_E).

The version of Space Weather Modeling Framework (SWMF) is currently used by NOAA's Space Weather Prediction Center is of particular interest because it produces surface disturbance outputs as part of magnetic disturbance forecasts. The SWMF is a software system (http://csem.engin.umich.edu/swmf) that simulates the space-weather environment from the solar chromosphere to the Earth's upper atmosphere [*Tóth et al.*, 2005]. The SWMF comprises physical processes in different space domains through a modular approach, i.e. each domain is covered by a numerical sub-model developed specifically for that purpose. The near-Earth space is divided into the following physical domains: global magnetosphere (GM), inner magnetosphere (IM), and ionosphere (IE). The GM part is based on MHD equations. In the IM area the bounce-averaged trajectories of electrons and ions of different energies are calculated to capture ring current dynamics. The IE region 3D sub-model considers ionization, recombination, ion-neutral friction, and various heat sources to simulate the interaction between the ionosphere and magnetosphere. The SWMF simulation provides, in particular, the virtual ground magnetograms calculating Biot–Savart contributions from the currents in the magnetosphere outside of $2.5R_E$, FACs between 110 km altitude and $2.5R_E$, and height-integrated Pedersen and Hall ionospheric currents [*Rastätter et al.*, 2014]. The SWMF consists of a dozen physics domains and sub-models and contains > 1 million lines of Fortran/C++ code, dozens of scripts and visualization tools (http://csem.engin.umich.edu/tools/swmf) [*Tóth et al.*, 2005]. The SWMF runs can be requested via the Community Coordinated Modeling Center at the NASA Goddard Space Flight Center (https://ccmc.gsfc.nasa.gov) [*Pulkkinen et al.*, 2009].

Here we present some results from [*Pilipenko et al.*, 2023] obtained with a version of SWMF that is currently in use to issue short-term space weather predictions [*Pulkkinen et al.*, 2013]. It is important to understand how well this model can capture ULF variations that drive GICs. The geomagnetic disturbances and associated bursts of GIC in the electric power line along Kola Peninsula for the May 27–28, 2017, geomagnetic storm were considered. The observations were compared with the global modeling results to validate whether this version of SWMF can reproduce adequately the magnetic field variability dB/dt, which is the driver of recorded GIC.

Comparison of Observations With the SWMF Modeling

The SWMF modeling output was obtained in the GSM coordinate system, where X is the coordinate along the Earth-Sun line directed towards the Sun. The model 1 run was performed with ~ 2 million grid cells with resolution $1/4\,R_E$ in the region $-20R_E \le X \le 8R_E$ and $|Y|, |Z| \le 8R_E$), but it had a finer resolution $1/8\,R_E$ near the Earth up to $3.5R_E$. The model 2 run was performed with ~ 9.6 million cells and had $1/4\,R_E$ resolution within $8R_E$, but it used $1/2\,R_E$ resolution in a large area further away from the Earth.

A system to monitor the GIC in power transmission line "Northern Transit" operates at the Kola Peninsula [*Selivanov et al.*, 2023]. The system consists of 4 substations at 330 kV power line. Each substation records a quasi-DC current in the dead-grounded neutral of the transformer. For the analysis data from the terminal substation Vykhodnoi (VKH) has been used with cadence from 2 Hz to 1-min.

The variations of the geomagnetic field horizontal components are measured by IMAGE magnetometers with 1-sec time resolution. The locations of selected magnetic stations in the vicinity of GIC recording system are shown in Figure 1. The substation VKH is located at the same geomagnetic latitude as magnetic stations IVA and LOZ.

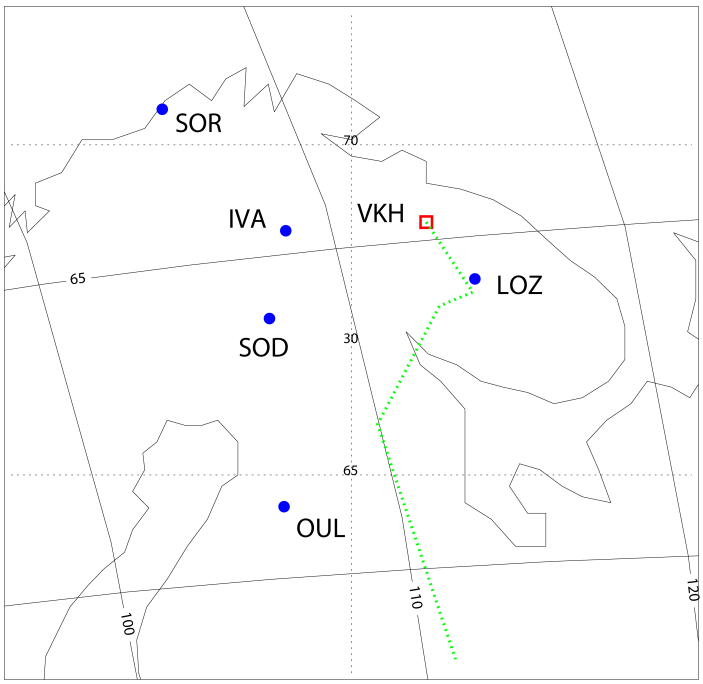

Figure 1. The map with location of GIC recording substation (empty red square) and nearby IMAGE magnetometers (blue dots). Solid thin lines denote the geomagnetic coordinates, dotted lines denote the geographic coordinates. The "Northern Transit" power transmission line is denoted by the dashed green line.

The SWMF modeling provides the horizontal magnetic field perturbation on the ground in the North, ΔB_n, and East, ΔB_e, directions with 1-min time resolution. The actual magnetometer observations at key station IVA from the IMAGE array have been compared with the same virtual station. Magnetic disturbances in the horizontal X and Y components, and time derivatives dX/dt, dY/dt, and $|d\mathbf{B}/dt| = \sqrt{(dX/dt)^2 + (dY/dt)^2}$, calculated with 3-point scheme, have been examined.

The storm on May 27, 2017, has been considered as an example. The storm was caused by the southward reorientation of IMF B_z at ~ 2130 UT. The extreme value of the *SYM-H* index was about −140 nT, and the auroral SML index irregularly decreased till about −1500 nT. Upon long-time growth phase the magnetic variations became irregular, when intense Pi3 pulsations superposed the magnetic bay during 00–05 UT, May 28 (Figure 2). These pulsations are quasi-periodic sequence of magnetic impulses, whose time scale varies from ~ 20 min to ~ 10 min, and are evident in all components, but most clearly in Y-component with peak-to-peak amplitudes ~ 300 nT.

Observations have been compared with the global magnetospheric parameters reproduced by modeling. The basic features of the *SYM-H* index characterizing the intensity of the ring current agreed with the modeling predictions (Figure 3). Although the extreme value of modeled *SYM-H* index, about −80 nT (model 2), was noticeably weaker than the measured *SYM-H* index. The SWMF model reproduces cross-polar potential *CP* index [kV]. For validation of the modeling results, a measure of the trans-polar current across the polar cap – the *PC* index [mV/m], has been used. The comparison indeed showed an expected similarity in variations of the modeled *CP* index and the *PC* index in both Northern and Southern hemispheres (Figure 3).

The main interest is whether modeling can describe not only global variations of the magnetosphere-ionosphere system, but the magnetic field variability as well. Although the magnetic disturbance was observed to be much larger in the X-component than in the Y-component, $|\Delta X| \gg |\Delta Y|$, the time derivatives dX/dt and dY/dt were nearly of the same peak-to-peak magnitude ~ 20 nT/s (Figure 2). During the period with high Pi3 activity, extremely high values of GIC amplitudes were recorded (peak-to-peak values up to J ~ 80 A) at the substation VKH (Figure 2). Each burst of magnetic variability was accompanied by a burst of GIC.

The virtual magnetograms for station IVA are shown in Figure 4. The modelled magnetic bay in the X-component roughly matched observations. The substorm onset on 22 UT, May 27 was well reproduced by modeling, although the magnetic disturbance was weaker than the observed one. However, the intense quasi-periodic pulsations in Y-

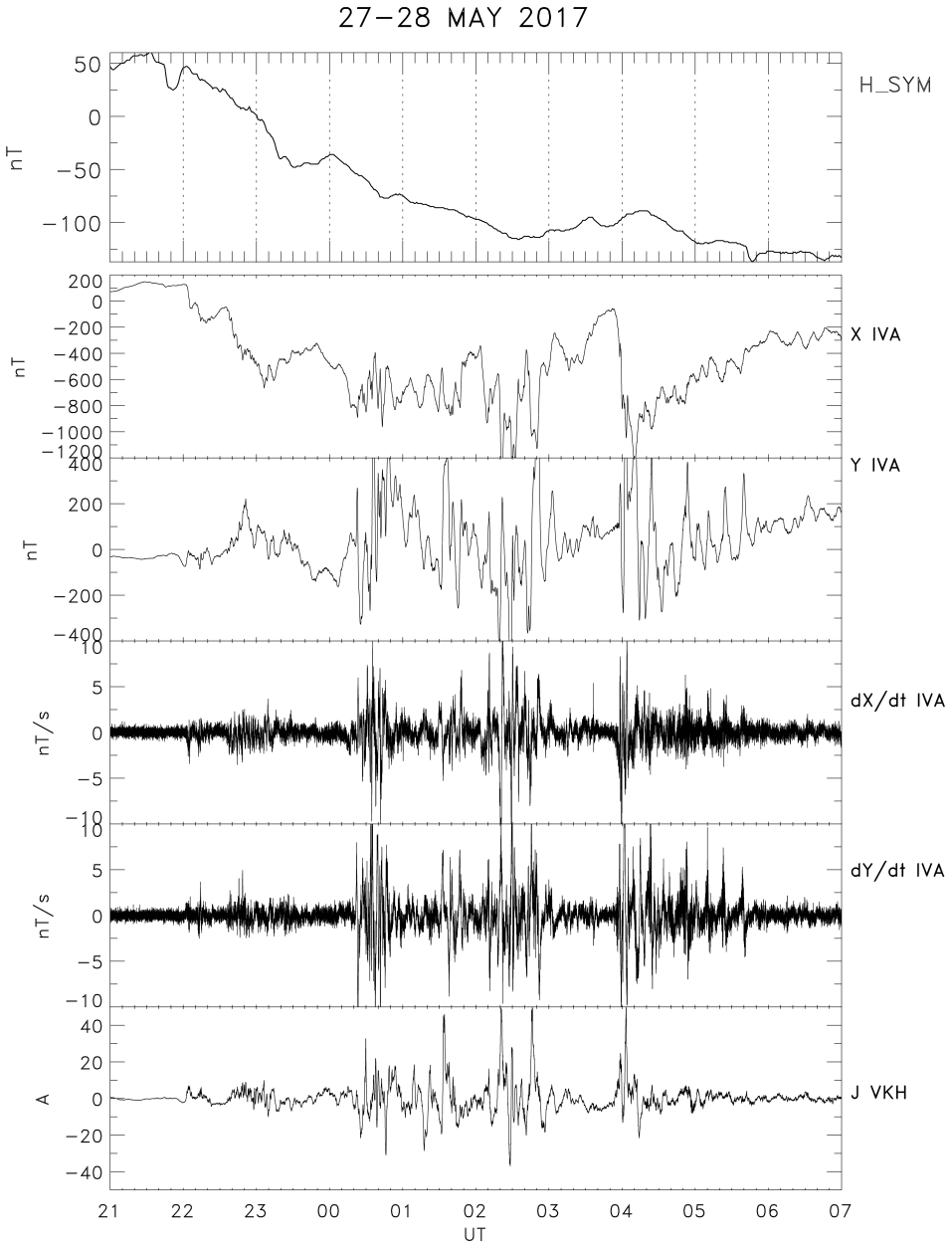

Figure 2. Variations during time interval 2017, May 27, 21 UT – May 28, 07 UT of the *SYM-H* index, geomagnetic field X and Y components at magnetic station IVA (1 Hz sampling rate); corresponding magnetic field variability (dX/dt, dY/dt), and GIC J recorded at VKH station (2 Hz sampling rate).

component did not show up in virtual magnetograms. The variability magnitude $|d\mathbf{B}/dt|$ predicted by the SWMF reached up to 10 nT/min only, that was much less than actual observations, ~ 200–300 nT/min300 (Figure 4). So, the contrast between the magnetic field variability predicted by the MHD modeling and observed fluctuations in Pi3 band was very prominent, more than an order of magnitude. Thus, the modeling of meso-scale magnetic field features was inadequate to predict the GIC magnitude in this event.

Restoration of Meso-Scale Ionospheric Vortex Characteristics From Ground Magnetometer Data

Standard data analysis tools for ULF waves based on the decomposition in time-space into a set of sinusoidal harmonics and plane waves cannot be applied for the analysis of impulsive disturbances. Pi3 time series is probably composed from hierarchy of vortices driven by localized FACs. The FAC flowing along the magnetic field lines between the mag-

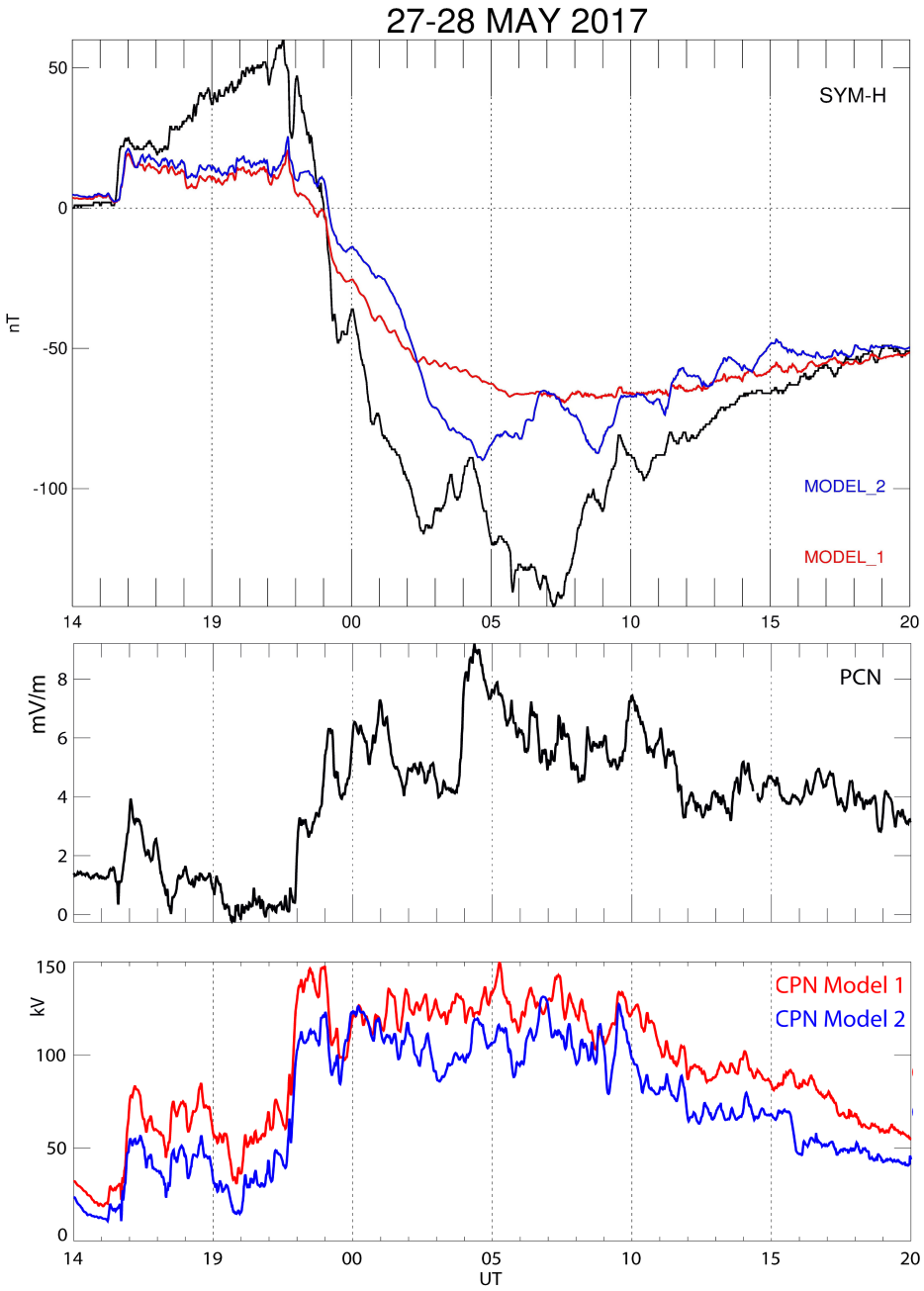

Figure 3. Variations during time interval 2017, May 27, 14 UT – May 28, 20 UT of the observed *SYM-H* index (black line) and the *SYM-H* index predicted by the SWFM modeling (runs 1 and 2 shown by red and blue lines), and of *PC* index [mV/m] (characterizing the intensity of the trans-polar current) in the Northern hemisphere (upper panel), and the modeled (run 1 and 2) cross-polar potential CPN in the Northern hemisphere [kV] (bottom panel).

netosphere and ionosphere is closed in the conducting E-layer by the system of transverse Pedersen $\mathbf{J}_P$ and Hall $\mathbf{J}_H$ currents

$$\mathbf{J}_\perp = \mathbf{J}_P + \mathbf{J}_H = \Sigma_P \mathbf{E} + \Sigma_H [\mathbf{n} \times \mathbf{E}].$$

Here, $\mathbf{J}_\perp$ is the height-integrated ionospheric current, $\mathbf{E}$ is the horizontal electric field, $\mathbf{n}$ is the normal to the ionospheric plane, and the Σ_P and Σ_H are height-integrated Pedersen and Hall conductances, $\mathbf{J}_P$ and $\mathbf{J}_H$ are the vortex-free (solenoidal) and divergence-free (eddy) components of the horizontal current vector $\mathbf{J}_\perp$. Introducing 2D differential

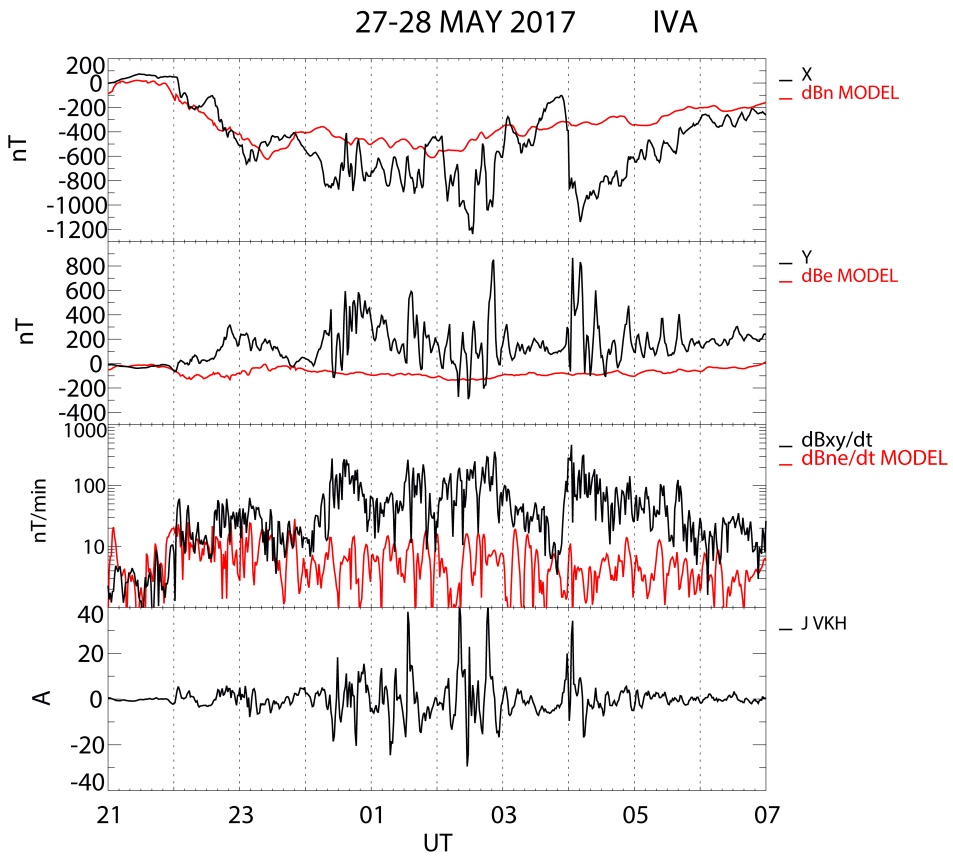

Figure 4. Variations of geomagnetic field and GIC during time interval 2017, May 27, 21 UT – May 28, 07 UT: (upper panels) magnetograms X, Y (black lines), measured at magnetic station IVA, and Bn, Be components predicted by SWMF model-1 for the same location (red line); (3rd panel) $|d\mathbf{B}/dt|$ estimated at IVA from data (black line) and from virtual magnetometer (red line); (bottom panel) GIC recorded at VKH substation.

operators Rot = $\mathbf{n}\cdot$ rot and Div = $\{\partial x, \partial y\}$ these properties can be written as Rot$\mathbf{J}_P = 0$ and Div$\mathbf{J}_H = 0$. At high latitudes, where the geomagnetic field is nearly vertical, the vertical current j_z is closed only by the Pedersen current $j_z = \text{Div}\mathbf{J}_P$. The total magnetic effect under the ionosphere from j_z and $\mathbf{J}_P$ vanishes, therefore the ground magnetic disturbance is produced only by $\mathbf{J}_H$. In the ionosphere with horizontally homogeneous conductance the local FAC is related to the current Hall as follows:

$$j_z = \left(\frac{\Sigma_P}{\Sigma_H}\right)\text{rot}\,\mathbf{J}_H.$$

An ionospheric vortex system is driven by local FAC (Figure 5, upper panel). The radial structure of the horizontal $B_r(r)$ and vertical $B_z(r)$ components of the magnetic field produced on the ground by such a system is qualitatively demonstrated in Figure 5 (bottom panel). Pedersen currents flow symmetrically from the center of the FAC tube, and they do not excite a magnetic response on the ground ($B_\varphi = 0$). The radial component $B_r(r)$ on the ground produced by the ionospheric Hall currents has a bipolar form ($B_r(r) \to 0$ under the center of the eddy current system) with maximum at distance $R_{\max}$. According to theoretical notions the corresponding radius δ of the ionospheric Hall current vortex is to be related with $R_{\max}$ as follows $\delta = \sqrt{2}R_{\max} - h$ (where h is the height of the E-layer).

For the analysis of magnetometer data from a 2D array a new technique was proposed in [*Chinkin et al.*, 2020]. Using the cubic polynomial interpolation, the observed values have been transformed onto a regular geographic 2D grid. To make the vortex-like structures

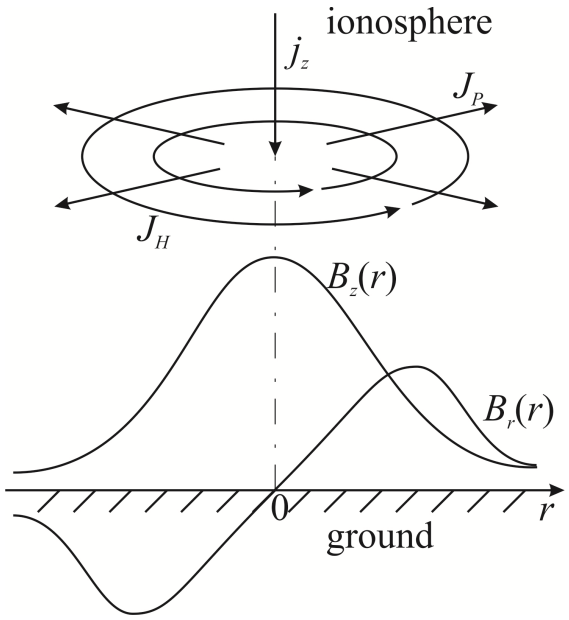

Figure 5. Schematic representation of the azimuthally symmetric field-aligned current J_z flowing into the ionosphere and its coupling to the transverse Pedersen J_P and Hall J_H currents in the conductive E-layer of the ionosphere (upper panel). Bottom panel shows radial dependence of the radial $B_r(r)$ and vertical $B_z(r)$ components of the geomagnetic disturbance on the ground.

more evident, the equivalent ionosphere current field $\mathbf{J}_\perp$ is derived by $\pi/2$ rotation of the ground field vector $\mathbf{B}_\perp$. Then, the 2D scalar field of the ionospheric current vorticity $G(x,y) = \mathrm{rot}\mathbf{J}_\perp(x,y)$ has been calculated. The extrema of function $G(x,y)$ correspond to FAC peaks flowing in or out the ionosphere. As a result, this technique enables one to determine a set of instant vortex centers $\mathbf{r}_0 = (x_0, y_0)$ for each time moment. A characteristic scale of vortex will be characterized by its effective radius R. The vortex radial scale is estimated by finding first significant extremum of vector circulation $\mathbf{J}_\perp$ along the contour $\Gamma(R)$ (the circle of radius R with its center at $\mathbf{r}_0$) $C(\Gamma(R)) = \oint_\Gamma \mathbf{J}\perp d\mathbf{l} = \int_S \mathrm{rot}\ \mathbf{J}_\perp dS$. To have the possibility to trace the vortex trajectory, the program merges automatically all the predetermined vortex centers, providing a possibility to determine a single vortex trajectory.

The developed algorithm was applied to identify a spatial structure of Pi3 pulsations during the magnetic storm on June 27–29, 2013 [*Chinkin et al.*, 2021]. The prolonged period of southward IMF drove the magnetosphere into the magnetic storm, during which geomagnetic indices reached maximal values of $|Dst| \sim 120$ nT and $AE \sim 1000$ nT. During the period when intense Pi3 pulsations were superposed on the magnetic bay (Figure 6), extremely high values of GICs were recorded (up to ~ 120 A per node) in transformers of power transmission line in North-West Russia [*Apatenkov et al.*, 2020; *Belakhovsky et al.*, 2019].

Data from 2D array of IMAGE magnetometers in the vicinity of the power line was analyzed. The snapshot of ionospheric Hall currents clearly shows the pair of FACs forming adjacent vortices (Figure 7). There is likely a hierarchy of such short-lived vortices with different spatial scales.

Figure 8 presents the time evolution of the vortex characteristics restored with the help of the described algorithm. The presented features include trajectories of the identified vortices (geographic latitude Φ and longitude Λ), FAC density J_z in the center of each vortex, and its estimated radius δ in the ionosphere. During the period 01–03 UT, the occurrence of irregular series of magnetic pulses is evident from magnetograms of Y and Z components (3rd and 2nd panels from the bottom in Figure 8). The peak values of J_z correspond to extrema of vertical Z component in accordance with the structure of an isolated vortex (Figure 5). Each magnetic pulse is found to be associated with the ionospheric vortex. Peak values of FAC density reach $|J_z| \sim 5\,\mathrm{A/km^2}$. Typical scale 2δ of the recognized vortices is ~ 400–500 km. The vorces move eastward, that is in the anti-sunward direction, and no regular movement in the latitudinal direction is observed. The observed pattern of vortices is compared with bursts of GICs recorded at VKH (bottom panel in Figure 8). The one-to-one correlation between a disturbance of component Z and GIC burst is clearly observed. Thus, each vortex induces a GIC enhancement with amplitude up to ~ 100 A.

GIC-effectiveness of CME and CIR Storms

Magnetic storms are caused by two possible forms of the solar activity. At the solar cycle maximum, non-recurrent storms caused by Coronal Mass Ejections (CMEs) are predominantly observed. At the minimum and declining phase of the solar activity, recurrent storms produced by high-speed solar wind streams emanating from coronal holes (Corotating Interaction Regions, CIR) are usually observed. CIRs cause magnetic storms of weak to moderate intensity, but these storms have a longer duration than CME storms. CIR storms develop against the background of fast-speed solar wind flows and

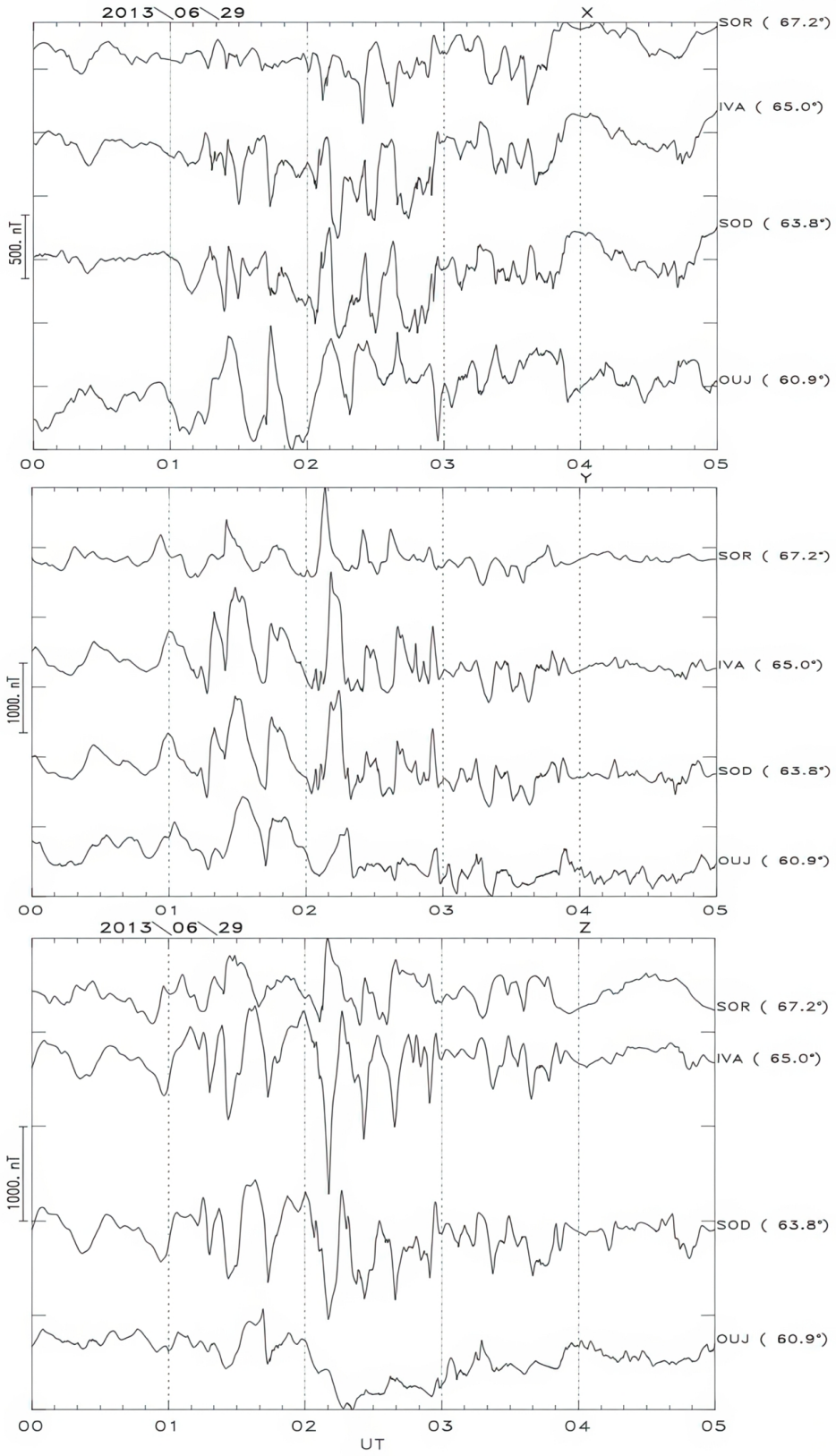

Figure 6. Geomagnetic field variations at latitudinal array of stations SOR, IVA, SOD, OUJ from the IMAGE array during magnetic storm on June 29, 2013, from 00 UT till 05 UT: X, Y, and Z components. Geomagnetic latitudes are indicated near the station codes on the right-hand ordinate axis.

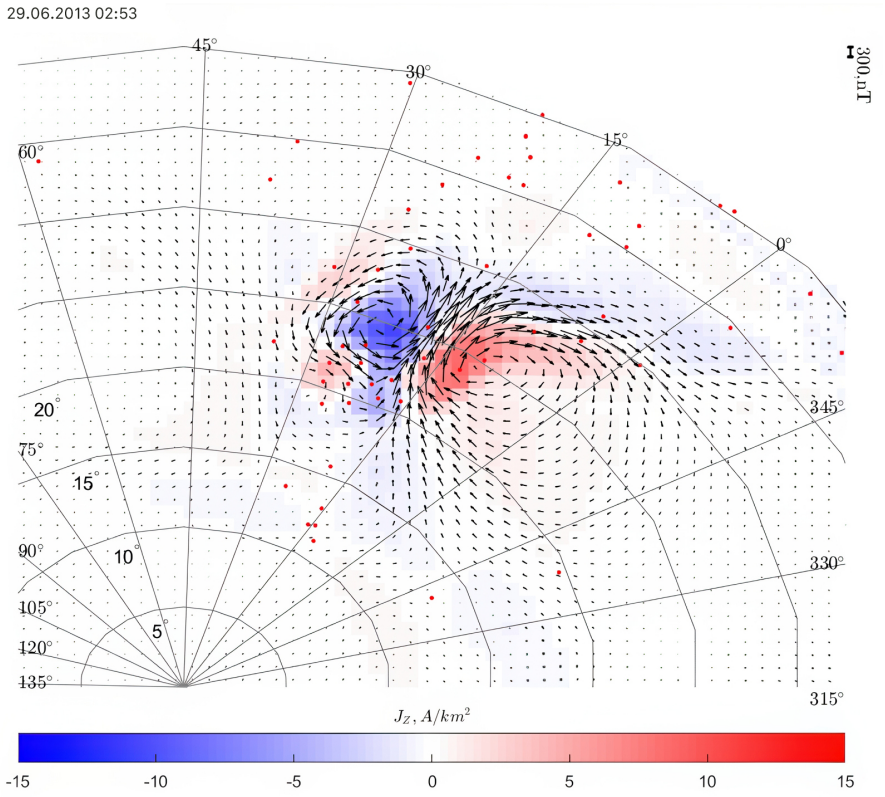

Figure 7. 2D vector field of the equavalent ionospheric current **J**, constructed for the time moment June 29, 0253 UT, 2013. Arrow length corresponds to the magnitude of ground magnetic disturbances. Red dots denote the station locations. The density of inward flowing FAC J_z>0 (corresponding to clockwise vortex) is denoted with red color, whereas the density of outward flowing FAC J_z<0 (corresponding to counterclockwise vortex) is denoted with blue color.

are accompanied by a higher level of ULF pulsations in the magnetosphere [*Borovsky and Denton*, 2006]. Naturally, the question arises about the generation efficiency of intense GICs by different types of magnetic storms. The impact of two types of magnetic storms on the growth of GICs in the power transmission line "Northern Transit" was considered in [*Belakhovsky et al.*, 2023] using as example the events on November 3–5, 2021 and October 11–13, 2021 (Figure 9).

The CME storm on November 3–5, 2021 is caused by the arrival of an interplanetary magnetic cloud to the Earth's magnetosphere. The *Dst/SYM-H* and *AE* indices reach −105/118 nT and ~ 3040 nT, correspondingly. The geomagnetic field disturbance in the vicinity of GIC recording substation is ΔX ~ 1200 nT (Figure 9, left-hand panel). The magnitude of the geomagnetic field time derivative reach $|dX/dt| \approx |dY/dt| \approx 300$ nT/min. The highest GIC magnitude at VKH substation is ~ 20 A.

The CIR magnetic storm on October 11–13, 2021 produces *Dst/SYM-H* up to −65/72 nT and *AE* index up to ~ 2650 nT. The IMF Bz component changes its sign to positive several times, which results in a low storm intensity. Three consecutive substorms observed at 19–23 UT, 23–02 UT, and 02–05 UT, are accompanied by GIC bursts (Figure 9, right-hand panel). The third substorm is the most intense ($\Delta X \approx 1000$ nT), while the GIC also reaches the highest magnitude ~ 40 A. The peak magnitudes of time derivatives are $|dX/dt|$ ~ 300 nT/min, and $|dY/dt|$ ~ 330 nT/min.

Geoeffectiveness of a magnetic storm in respect to the GIC excitation may be characterized by the ratio between the maximal $|SYM-H|_{\max}$ and maximal GIC amplitude $J_{\max}$

$$\Gamma = J_{\max}/|SYM-H|_{\max}.$$

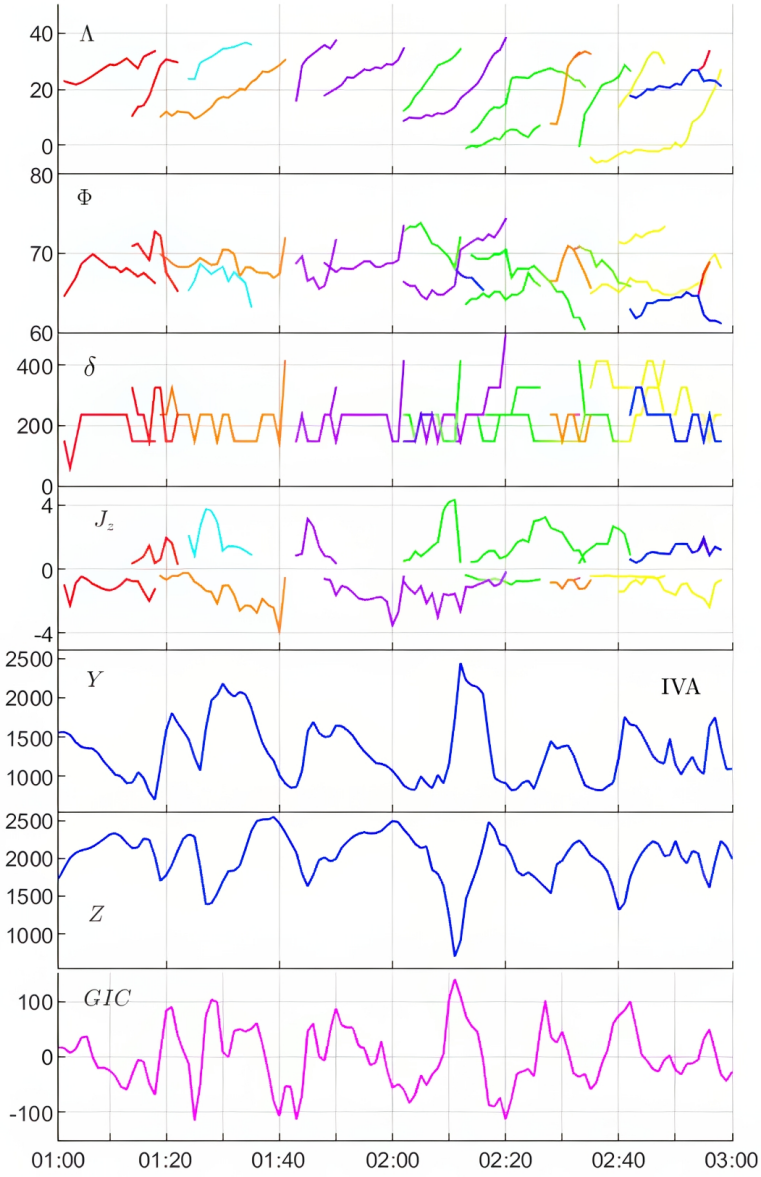

Figure 8. Dynamics of the vortex characteristics during time interval June 29, 2013, from 01 to 03 UT (from top to bottom): geographic longitude Λ and latitude Φ of the vortex center, radial scale δ [km] of each vortex in the ionosphere, and density of FAC J_z [A/km^2] in the vortex center. Bottom panels show the variations of Y [nT] and Z [nT] components of geomagnetic field at IVA station, and GIC [A] recorded in the transformer at substation VKH. The ratio Σ_P/Σ_H has been set equal 1.

The CME storm on November 2021 has $J_{\max}$ ~ 20 A, whereas the CIR storm on October 2021 has maximal recorded GIC magnitude $J_{\max}$ ~ 40 A. Thus, the GIC-effectiveness of the CME storm is Γ = 0.17 A/nT, and that of the CIR storm is Γ = 0.56 A/nT, thus nearly 3 times larger! The comparison of storm geoeffectiveness according to maximal *AE* index provides a similar difference, but ~ 2.5 times.

The reason for this difference can be comprehended by consideration of 2D distribution of ionospheric currents for both storms constructed from 2D magnetometer array (Figure 10). For the CME storm at the time of GIC maximum (2135 UT), a predominant contribution to geomagnetic disturbances is provided by the westward auroral electrojet. For the CIR storm at the moment of GIC maximum (0315 UT), along with the auroral electrojet, a significant contribution of eddy current systems to geomagnetic disturbances is observed.

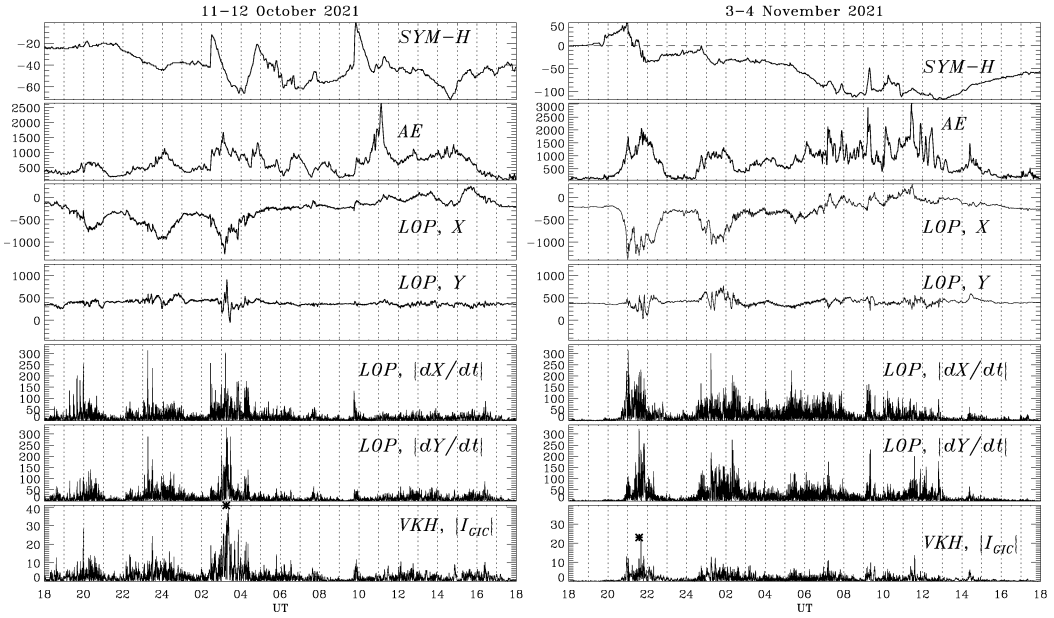

Figure 9. Variations of geomagnetic field at LOP station and GIC during the CME storm on November 3, 18 UT – November 4, 18 UT, 2021 (left-hand panel) and CIR storm on October 11, 18 UT – October 12, 18 UT, 2021 (right-hand panel): *SYM-H* index [nT], *AE* index [nT], X and Y-components of the geomagnetic field [nT], magnitudes |dX/dt| [nT/min] and |dY/dt| [nT/min], and GIC amplitude J [A] from VKH substation.has been set equal 1.

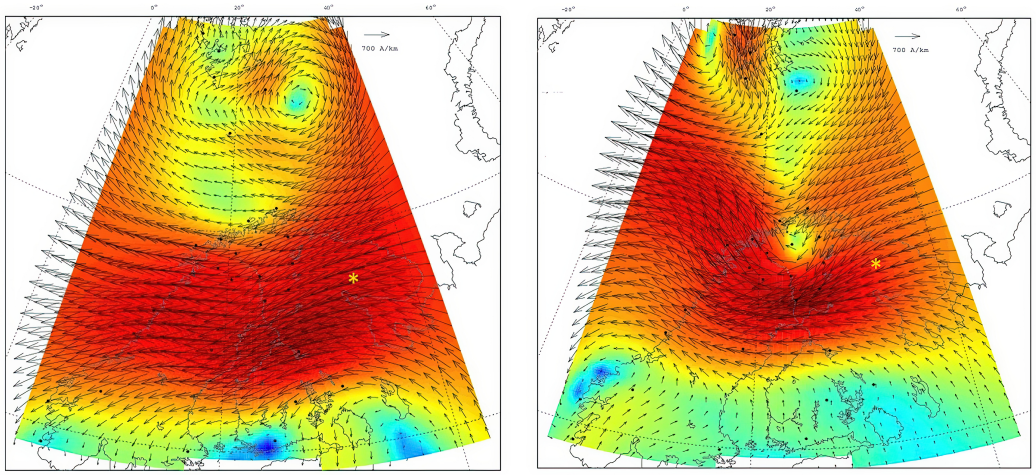

Figure 10. Equivalent ionospheric current systems according to 2D IMAGE magnetometer array for November 3, 2021, 21:35 UT (left-hand panel) and for October 12, 2021, 03:15 UT (right-hand panel). Yellow star indicates the location of GIC substation VKH.

Thus, GIC magnitude does not always depend on the storm intensity only. Development of eddy ionospheric current systems can lead to a significant GIC for weaker CIR storms. However, the reliable prediction of the space weather impact on technological systems is still a challenge for the space community because we still cannot predict the occurrence of vortex structures during a particular storm.

Prospects of Future Studies

Some studies that compared magnetometer measurements with simulated ground magnetic fields with various global MHD models [*Kwagala et al.*, 2020; *Yu and Ridley*, 2008] indicated that observational data contain more structure than a model, and a model tends to miss some localized intense disturbances. In general, most of the models tend

to underestimate the dB/dt [*Pulkkinen et al.*, 2013]. Therefore, continual investigation of global models with new events is highly beneficial to obtain a greater understanding of the model applicability for space weather purposes. Any efforts to compare the global MHD modeling results with actual GIC observations, but not just GIC proxy dB/dt, are highly desirable.

The analysis of the geomagnetic disturbances and GIC variations during the magnetic storm on May 2017 showed that the evolution of global magnetospheric parameters was reasonably well reproduced by the SWMF modeling. However, the current version of SWMF was found to be unable to reproduce the meso-scale ionospheric structures (few hundred km) [*Pilipenko et al.*, 2023]. Comparison of IMAGE magnetometer observations during the September 2017 storm with virtual magnetometers from the SWMF run for various spatial resolutions, from low ($1/4R_E$ and 10^6 cells) to high ($1/16R_E$ and 8×10^6 cells), showed that only at low/mid-latitudes a higher spatial resolution provided more accurate magnetic disturbances, whereas at sub-auroral latitudes, increasing the spatial resolution provided a negligible improvement [*Dimmock et al.*, 2021]. In a similar way, investigation of the SWMF performance in predicting magnetic perturbations for major storms in 2001–2015 showed that modeling captured only the general trend of ground perturbations [*Kwagala et al.*, 2020]. The model performed reasonably well for dB/dt predictions for the low level < 60 nT/min, but short-lived large dB/dt were greatly underestimated. These facts suggest that global MHD models used for space weather predictions are inadequate so far for the prediction of intense GIC bursts related to Pi3 pulsations and other meso-scale structures.

The low-frequency part of the ULF period range (5–20 min) is of special importance for the GIC studies. While the spectral power of geomagnetic variations in general drops with frequency, the magnetic field variability dB/dt grows with frequency. The resultant GIC is the convolution of these factors and has a maximum at time scales 2–10 min, that is in the period range of Pi3 pulsations. At these regional scales, weaker but rapidly varying localized vortex-like current systems superposed on the electrojet produce intense GIC bursts. The new technique of data analysis has confirmed that actual driver of GIC is not the intensification of global ionospheric electrojet, but the occurrence of meso-scale short-lived structures in the ionosphere. Bursts of largest GICs is caused by a quasi-periodic sequence of local anti-sunward drifting ionospheric vortices driven by FACs with densities up to ~ 5×10^{-6} A/m^2. It is hard to decide whether the inability of the SWMF to predict the occurrence of Pi3 pulsations is related with some missing magnetotail physics or not, because the physical mechanism of these pulsations has not been firmly established yet. Pi3 pulsation periodicity (5–20 min) is longer than typical magnetospheric field line eigenoscillations (~ 3 min). Thus, though Pi3 pulsations are mentioned in all the textbooks on ULF waves in the magnetosphere, their physical mechanism is still a challenge to the ULF community. The relationship between the large-scale auroral electrojet and localized current systems superposed on it has not been established yet.

Rather unexpectedly, weaker CIR storms were found to produce more intense GIC bursts than stronger CME storms. This distinction is caused by a higher level of Pi3 pulsations during the CIR storms. Thus, the fine impulsive structure of storm/substorm seems to be important, but underestimated, factor of the space weather geoeffectiveness. Although, many additional factors, such as the underlying crust conductivity, configuration of the power transmission system, type of high-voltage transformer, etc. are also essential for the GIC size in a particular system.

Acknowledgments. The SWMF modeling results were provided by L. Rastaetter and M. Hartinger. We appreciate a very thorough examination of the m/s by a Reviewer and his helpful comments. The study is supported by the grant 21-77-30010 from the Russian Science Foundation. The IMAGE magnetometer data and related 2D ionospheric current modeling are available at the website https://space.fmi.fi/image/.

References

Amm, O., and A. Viljanen (2014), Ionospheric disturbance magnetic field continuation from the ground to the ionosphere using spherical elementary current systems, *Earth, Planets and Space*, *51*(6), 431–440, https://doi.org/10.1186/BF03352247.

Apatenkov, S. V., V. A. Pilipenko, E. I. Gordeev, et al. (2020), Auroral Omega Bands are a Significant Cause of Large Geomagnetically Induced Currents, *Geophysical Research Letters*, *47*(6), https://doi.org/10.1029/2019GL086677.

Belakhovsky, V. B., V. Pilipenko, M. Engebretson, et al. (2019), Impulsive disturbances of the geomagnetic field as a cause of induced currents of electric power lines, *Journal of Space Weather and Space Climate*, *9*, https://doi.org/10.1051/swsc/2019015.

Belakhovsky, V. B., V. A. Pilipenko, Y. A. Sakharov, and V. N. Selivanov (2023), The Growth of Geomagnetically Induced Currents during CME and CIR Geomagnetic Storms in 2021, *Bulletin of the Russian Academy of Sciences: Physics*, *87*(2), 236–242, https://doi.org/10.3103/S1062873822700988.

Borovsky, J. E., and M. H. Denton (2006), Differences between CME-driven storms and CIR-driven storms, *Journal of Geophysical Research: Space Physics*, *111*(A7), https://doi.org/10.1029/2005JA011447.

Chinkin, V. E., A. A. Soloviev, and V. A. Pilipenko (2020), Identification of Vortex Currents in the Ionosphere and Estimation of Their Parameters Based on Ground Magnetic Data, *Geomagnetism and Aeronomy*, *60*(5), 559–569, https://doi.org/10.1134/S0016793220050035.

Chinkin, V. E., A. A. Soloviev, V. A. Pilipenko, et al. (2021), Determination of vortex current structure in the high-latitude ionosphere with associated GIC bursts from ground magnetic data, *Journal of Atmospheric and Solar-Terrestrial Physics*, *212*, 105,514, https://doi.org/10.1016/j.jastp.2020.105514.

Dimmock, A. P., D. T. Welling, L. Rosenqvist, et al. (2021), Modeling the Geomagnetic Response to the September 2017 Space Weather Event Over Fennoscandia Using the Space Weather Modeling Framework: Studying the Impacts of Spatial Resolution, *Space Weather*, *19*(5), https://doi.org/10.1029/2020SW002683.

Engebretson, M. J., K. R. Kirkevold, E. S. Steinmetz, et al. (2020), Interhemispheric Comparisons of Large Nighttime Magnetic Perturbation Events Relevant to GICs, *Journal of Geophysical Research: Space Physics*, *125*(8), https://doi.org/10.1029/2020JA028128.

Gombosi, T. I., Y. Chen, A. Glocer, et al. (2021), What sustained multi-disciplinary research can achieve: The space weather modeling framework, *Journal of Space Weather and Space Climate*, *11*, 1–55, https://doi.org/10.1051/swsc/2021020.

Heyns, M. J., S. I. Lotz, and C. T. Gaunt (2021), Geomagnetic Pulsations Driving Geomagnetically Induced Currents, *Space Weather*, *19*(2), https://doi.org/10.1029/2020SW002557.

Kappenman, J. G. (2005), An overview of the impulsive geomagnetic field disturbances and power grid impacts associated with the violent Sun-Earth connection events of 29-31 October 2003 and a comparative evaluation with other contemporary storms, *Space Weather*, *3*(8), https://doi.org/10.1029/2004SW000128.

Kozyreva, O., V. Pilipenko, R. Krasnoperov, et al. (2019), Fine structure of substorm and geomagnetically induced currents, *Annals of Geophysics*, *62*, https://doi.org/10.4401/ag-8198.

Kwagala, N. K., M. Hesse, T. Moretto, et al. (2020), Validating the Space Weather Modeling Framework (SWMF) for applications in northern Europe: Ground magnetic perturbation validation, *Journal of Space Weather and Space Climate*, *10*, 33, https://doi.org/10.1051/swsc/2020034.

Morley, S. K. (2020), Challenges and Opportunities in Magnetospheric Space Weather Prediction, *Space Weather*, *18*(3), https://doi.org/10.1029/2018SW002108.

Ngwira, C. M., D. Sibeck, M. V. D. Silveira, et al. (2018), A Study of Intense Local dB/dt Variations During Two Geomagnetic Storms, *Space Weather*, *16*(6), 676–693, https://doi.org/10.1029/2018SW001911.

Pilipenko, V. A. (2021), Space weather impact on ground-based technological systems, *Solar-Terrestrial Physics*, *7*(3), 68–104, https://doi.org/10.12737/stp-73202106.

Pilipenko, V. A., O. Kozyreva, M. Hartinger, et al. (2023), Is the Global MHD Modeling of the Magnetosphere Adequate for GIC Prediction: the May 27-28, 2017 Storm, *Cosmic Research*, *61*(2), 120–132, https://doi.org/10.1134/S0010952522600044.

Pirjola, R., K. Kauristie, H. Lappalainen, et al. (2005), Space weather risk, *Space Weather*, *3*(2), https://doi.org/10.1029/2004SW000112.

Pulkkinen, A., M. Hesse, M. Kuznetsova, and L. Rastätter (2007), First-principles modeling of geomagnetically induced electromagnetic fields and currents from upstream solar wind to the surface of the Earth, *Annales Geophysicae*, *25*(4), 881–893, https://doi.org/10.5194/angeo-25-881-2007.

Pulkkinen, A., M. Hesse, S. Habib, et al. (2009), Solar shield: forecasting and mitigating space weather effects on high-voltage power transmission systems, *Natural Hazards*, *53*(2), 333–345, https://doi.org/10.1007/s11069-009-9432-x.

Pulkkinen, A., L. Rastätter, M. Kuznetsova, et al. (2013), Community-wide validation of geospace model ground magnetic field perturbation predictions to support model transition to operations, *Space Weather*, *11*(6), 369–385, https://doi.org/10.1002/swe.20056.

Rastätter, L., G. Tóth, M. M. Kuznetsova, and A. A. Pulkkinen (2014), CalcDeltaB: An efficient postprocessing tool to calculate ground-level magnetic perturbations from global magnetosphere simulations, *Space Weather*, *12*(9), 553–565, https://doi.org/10.1002/2014SW001083.

Selivanov, V., T. Aksenovich, V. Bilin, et al. (2023), Database of geomagnetically induced currents in the main transmission line «Northern Transit», *Solar-Terrestrial Physics*, *9*(3), 93–101, https://doi.org/10.12737/stp-93202311.

Tóth, G., I. V. Sokolov, T. I. Gombosi, et al. (2005), Space Weather Modeling Framework: A new tool for the space science community, *Journal of Geophysical Research: Space Physics*, *110*(A12), https://doi.org/10.1029/2005JA011126.

Viljanen, A., and R. Pirjola (1994), Geomagnetically induced currents in the Finnish high-voltage power system: A geophysical review, *Surveys in Geophysics*, *15*(4), 383–408, https://doi.org/10.1007/BF00665999.

Yagova, N. V., V. A. Pilipenko, Y. A. Sakharov, and V. N. Selivanov (2021), Spatial scale of geomagnetic Pc5/Pi3 pulsations as a factor of their efficiency in generation of geomagnetically induced currents, *Earth, Planets and Space*, *73*(1), https://doi.org/10.1186/s40623-021-01407-2.

Yu, Y., and A. J. Ridley (2008), Validation of the space weather modeling framework using ground-based magnetometers, *Space Weather*, *6*(5), https://doi.org/10.1029/2007SW000345.

Zhang, J. J., C. Wang, and B. B. Tang (2012), Modeling geomagnetically induced electric field and currents by combining a global MHD model with a local one-dimensional method, *Space Weather*, *10*(5), https://doi.org/10.1029/2012SW000772.